Drug Design, Development and Therapy

Dovepress
Taylor & Francis Group

Open Access Full Text Article

ORIGINAL RESEARCH

Liu Wei Di Huang Decoction Alleviates Renal Fibrosis by Inhibiting Endothelial Mesenchymal Transitions via Upregulating Sirt1 Expression and Inhibiting the Wnt/β-Catenin Signaling Pathway

Hui Wang[1,2], Shuang-Shuang Chen[1], Yong-Xian Zhang[2], Hai-Bo Gao[1], Bin Meng[1], Wei-Yu Wu[1], Qun Tang[1]

[1]Medical School, Hunan University of Chinese Medicine, Changsha, 410208, People's Republic of China; [2]The 960th Hospital of the PLA Joint Logistics Support Force, Jinan, Shandong, 250000, People's Republic of China

Correspondence: Qun Tang, Medical School, Hunan University of Chinese Medicine, Changsha, 410208, People's Republic of China, Email tangqun460@126.com

Background: Renal fibrosis (RF) is the final outcome of chronic kidney disease (CKD), which can be triggered by various factors. Liuwei Dihuang Decoction (LWDHD) has been clinically established as an effective treatment for CKD, demonstrating anti-inflammatory, antioxidant, and antifibrotic effects. However, the specific molecular mechanisms underlying the therapeutic effectiveness of LWDHD remain unknown.

Aim: Prediction of key active ingredients, targets, and mechanistic pathways of LWDHD in RF treatment.

Materials and Methods: The bioactive components of LWDHD were identified and quantified using ultra-performance liquid chromatography-tandem quadrupole mass spectrometry (UHPLC-MS/MS). A network pharmacology approach was employed to predict the key targets of these bioactive components. A rat model of renal tubulointerstitial fibrosis was created through unilateral ureteral obstruction (UUO). Rats were divided into six groups: sham operation, UUO, low-dose LWDHD (LW-L), medium-dose LWDHD (LW-M), high-dose LWDHD (LW-H), and enalapril group. Continuous gavage of treatments was administered for 2 weeks. The renal tissues were histopathologically assessed, including HE, Masson's trichrome, and Sirius red staining, immunohistochemistry, co-staining and Western blot analysis to evaluate the effects of LWDHD on renal fibrosis. Transforming growth factor beta-1 (TGF-β1) was employed to stimulate endothelial-mesenchymal transition (EndMT) in EA.hy926 cells. The inhibitory effect of LWDHD on EndMT was validated through cellular morphology observations, Western blotting, and immunofluorescence assays.

Results: LWDHD showed promise as a therapeutic agent by alleviating renal pathological injury and lowering collagen fiber accumulation. It enhanced Sirt1 expression while inhibiting the Wnt/β-catenin signaling pathway. Moreover, LWDHD increased the levels of the endothelial marker CD31 and decreased the expression of fibrosis-associated proteins, such as α-smooth muscle actin (α-SMA) and vimentin, thereby mitigating renal fibrosis.

Conclusion: LWDHD has the potential to alleviate renal fibrosis, possibly through the upregulation of Sirt1, which inhibits the Wnt/β-catenin signaling pathway and thereby reduces EndMT.

Keywords: renal fibrosis, LWDHD, network pharmacology, Sirt1, Wnt/β-catenin, EndMT

Introduction

Worldwide, approximately 850 million individuals are affected by kidney-related disorders, including chronic kidney disease (CKD), acute kidney injury (AKI), and kidney failure.[1] The prevalence of CKD is rising globally and is projected to become the fifth leading cause of death by the year 2040.[2] CKD creates a significant economic strain on many families. Thus, implementing effective strategies to prevent both the initiation and progression of CKD is essential.

Received: 10 April 2025
Accepted: 13 July 2025
Published: 30 July 2025

Renal fibrosis (RF), which is triggered by various factors, represents the common pathological outcome of worsening CKD, and is a primary factor leading to end-stage renal failure.[3] RF encompasses glomerulosclerosis and renal tubulointerstitial fibrosis (RIF).[4] The characteristics of RIF are marked by the activation and proliferation of fibroblasts, as well as excessive deposition resulting from an imbalance in the degradation of extracellular matrix (ECM). Pathological changes encompass renal tubular injury, interstitial fibrosis, extensive infiltration of inflammatory cells, and increased collagen fiber deposition.[5] Numerous studies have demonstrated that during RIF, endothelial cells undergo endothelial-to-mesenchymal transition (EndMT), a specialized form of epithelial-mesenchymal transition (EMT).[6] During the EndMT process, a significant decrease occurs in the levels of endothelial cell-specific markers, including CD31, whereas a marked increase occurs in the expression of genes associated with mesenchymal characteristics, such as vimentin, α-smooth muscle actin (α-SMA), and fibroblast-specific protein-1 (FSP-1).[7,8]

The Wnt/β-catenin signaling pathway is pivotal in modulating renal EndMT progression.[9] Under normal physiological conditions, this pathway is quiescent in mature kidneys. However, it becomes aberrantly activated in various kidney diseases,[10] resulting in the increased expression of downstream genes including FSP-1, Collagen I, and vimentin.[11]

Sirtuins (Sirt1–7) are a family of NAD+-dependent histone deacetylases that regulate various physiological processes, including oxidative stress, fibrosis, apoptosis, and autophagy-related inflammation.[12] Studies demonstrated that Sirt6 deletion in proximal tubules activated the Wnt/β-catenin signaling pathway, thereby exacerbating UUO-induced tubulointerstitial inflammation and fibrosis.[13,14] Furthermore, Sirt6 inhibits the Wnt/β-catenin signaling pathway, which in turn blocks the renin-angiotensin system, thus preventing podocyte injury.[15] These findings suggested that sirtuins are intricately linked to the Wnt/β-catenin signaling pathway and play a critical role in combating renal fibrosis. Sirt1 deficiency markedly increases the levels of reactive oxygen species (ROS). Intracellular accumulation of ROS can induce inflammation,[16] damage nucleic acids, proteins, and lipids within cells; hence, maintaining the ROS balance is crucial for organismal homeostasis.[17] Wang Y focused on the damage to peritubular capillaries in the UUO model. Under ischemic and hypoxic conditions, renal endothelial cells undergo EndMT, Calcium dobesilate was shown to inhibit the progression of EndMT by activating p53 acetylation, suppressing apoptosis, and enhancing Sirt1 expression, thereby exerting a protective effect on the kidneys.[18] Notably, reduced Sirt1 expression can lead to the development of both acute and chronic nephropathies.[19,20] Therefore, investigating the mechanisms by which Sirt1 influences RIF holds substantial research value.

LWDHD was first mentioned in the "Key to Therapeutics of Children's Diseases" by Qian Yi during the Northern Song Dynasty. LWDHD possesses antioxidative, anti-inflammatory, and antifibrotic functions.[19] LWDHD, a classic herbal formula that has been widely utilized in China since the 11th century, is capable of nourishing the kidneys and has been effectively used for treating CKD in clinical practice.[20,21] LWDHD consists of *Rehmannia glutinosa Libosch, Dioscorea opposita Thunb, Cornus officinalis Sieb, Paeonia suffruticosa Andrews, Alisma orientale, and Poria cocos* in an 8:4:4:3:3:3 ratio.[22] LWDHD can help protect the kidneys through detoxification, turbidity removal, and renal deficiency tonification. Furthermore, numerous studies have demonstrated that various herbs, such as *Poria cocos*, can ameliorate both acute and chronic kidney injuries by modulating the Wnt/β-catenin signaling pathway.[23] Additionally, celastrol has been shown to alleviate fibrosis through the regulation of Sirt1 and Wnt/β-catenin signaling pathways.[24] Traditional Chinese medicine (TCM) has exhibited a multicomponent and multitarget therapeutic effect in the treatment of kidney diseases. The purpose of this study was to determine whether LWDHD can downregulate the Wnt/β-catenin signaling pathway by modulating Sirt1 expression, thus achieving antifibrotic effects.

Materials and Methods

Pharmaceutical Preparation

The active pharmaceutical ingredients contained in LWDHD are as follows: *Rehmannia glutinosa* Libosch 24 g, *Dioscorea opposita* Thunb 12 g, *Cornus officinalis* Sieb 12 g, *Paeonia suffruticosa* Andrews 9 g, *Alisma orientale* 9 g, and *Poria cocos* 9 g. The batch numbers used were 22042541C, CK22080807, SX1091205, NG22082302, 2207240122, and CK22082302, respectively. All components were procured from the First Affiliated Hospital of Hunan University of Chinese Medicine (Changsha, China). All components were subjected to two rounds of boiling,

followed by filtration and concentration, such that each 1 mL of the decoction contained approximately 2 g of each crude ingredient. Enalapril tablets were sourced from Yangtze River Pharmaceutical Group (batch number: 22030111).

UHPLC-MS/MS

The stationary phase used was a octadecylsilane-bonded silica gel (SinoChrom ODS2, dimensions 2.1×100 mm, particle size 1.8 μm; Dalian Elite Analytical Instruments Co., Ltd., Dalian, China). Methanol made up mobile phase A, whereas a 0.1% solution of formic acid made up mobile phase B. The flow rate was set at 0.3 mL/min, and the column temperature was maintained at 35 °C. Detection was performed using a quadrupole-time-of-flight mass spectrometer (model X 500R, AB SCIEX DISTRIBUTION, Coppell, TX, USA). To prepare the sample, 1 mL of the drug solution (0.1 g/mL) was placed into a 10-mL centrifuge tube and diluted with water until the final volume reached 10 mL. Following centrifugation at 12000r/min, the supernatant was collected. Precisely 10 μL of the prepared solution was injected into the liquid chromatography-mass spectrometry system for a 45-min analysis. The obtained data were compared with the retention times of standard compounds for network pharmacological analysis.[25]

Network Pharmacology

The active constituents within the LWDHD solution were identified through UHPLC-MS/MS analysis. The chemical profiles of six traditional Chinese medicinal herbs, *Rehmannia glutinosa Libosch, Dioscorea opposita Thunb, Cornus officinalis Sieb, Paeonia suffruticosa Andrews, Alisma orientale, and Poria cocos*, were retrieved from the TCMSP database (https://old.tcmsp-e.com/tcmsp.php). Using screening criteria of oral bioavailability (OB) ≥ 30% and drug-likeness (DL) ≥ 0.18, potential target genes for active compounds such as loganin, paeoniflorin, morroniside, and rehmannioside were sought in the GenCards database (https://www.genecards.org). After removing any redundancies, target genes were acquired from the UniProt protein database (https://www.uniprot.org).

To identify renal fibrosis-related targets, the GenCards and OMIM databases (https://omim.org) were queried using the term "Renal fibrosis" with filtering conditions set at "Relevance Score" ≥ 2 and "Gifts" ≥ 40. Duplicate entries were eliminated from the results. The active LWDHD components and renal fibrosis-associated targets were then cross-referenced using the Venny2.1 online tool (https://bioinfogp.cnb.csic.es/tools/venny/index.html), generating a map of intersecting targets. These intersecting targets were subsequently uploaded to the STRING11.5 platform (https://string-db.org), with the species specified as "Homo sapiens" and other parameters maintained at their default settings. A Protein-Protein Interaction (PPI) network diagram was generated and exported. The data were downloaded in TSV format and further analyzed using Cytoscape3.9.1 along with the CytoHubba plugin to pinpoint key core targets.[26] Using the degree topological algorithm, the top 20 critical targets were identified, with Sirt1 selected as the primary focus for follow-up research.

To gain deeper insights into the mechanisms by which LWDHD influences renal fibrosis, Gene Ontology (GO) functional analysis, encompassing biological processes (BP), molecular functions (MF), and cellular components (CC), and KEGG pathway enrichment analysis were performed using the DAVID database (https://david.ncifcrf.gov/).[27] This process elucidated the signaling pathways and molecular functions influenced by LWDHD. The enrichment analysis outcomes were visualized using the Microbiome platform. Additionally, molecular docking simulations between the LWDHD active components loganin, paeoniflorin, and morroniside and the core target Sirt1 were performed utilizing the AutoDock Tools-1.5.6 software.

Animals

Forty-eight male SPF-grade SD rats, weighing 200–220 g, were provided by Hunan Silek Jingda Laboratory Animal Co., Ltd. under the animal license number SCXK (Xiang) 2019-0004 and quality certification number ZS-202110120009. The study was conducted in accordance with the National Institutes of Health guidelines on the use of experimental animals. All experimental operations were approved by the Animal Ethics Committee of Hunan University of Chinese Medicine (ethical approval number LLBH-202205120006). Following a 1-week adaptation period at the Animal Center of Hunan University of Chinese Medicine, the rats were randomly allocated into six groups: sham operation, UUO, LW-L, LW-M, LW-H, and enalapril, with eight rats in each group. After being weighed, the rats were anesthetized via intraperitoneal injection of sodium pentobarbital (80 mg/kg) and positioned prone for

surgery. A 1.5-cm longitudinal incision was made 1.0 cm left of the spine and approximately 0.5 cm below the iliac crest. The ureter was isolated and two 4–0 surgical sutures were placed around it, one near the renal pelvis and the other approximately 1 cm away, which was then ligated and cut midway. For the sham operation group, all procedures were identical except that no ligation or ureter cutting was performed.[28] At 2 h after the procedure, the LW-L, LW-M, and LW-H groups received oral doses of 3.375, 6.75, and 13.5 g/kg, respectively, whereas the enalapril group received 10 mg/kg, based on human-to-rat dose conversion.[29] The UUO and sham operation groups were given equivalent volumes of normal saline orally. This dosing regimen was repeated daily for 14 d. At the conclusion of the experiment, the rats were euthanized through abdominal aortic blood collection under anesthesia. Their affected kidneys were excised and sectioned along the sagittal plane. One portion was fixed in 4% paraformaldehyde, whereas the cortical sections were stored in cryotubes for further analysis.

Renal Histopathological Analysis

The renal tissues were fixed with 4% paraformaldehyde, embedded in paraffin, and subsequently cut into 3-μm-thick sections for hematoxylin and eosin (HE) staining (Biosharp, Beijing, China). A pathologist assessed and scored tubule injury using a five-point grading system (0, normal; 1, <25%; 2, 25–50%; 3, 50–75%; and 4, ≥75%).[30] Masson trichrome staining (Servicebio, Wuhan, China) and Sirius Red staining (Kuai Mai, Hunan, China) were used to observe collagen fiber deposition. Collagen fibers were quantified using the ImageJ software (NIH, Bethesda, MD, USA), and the collagen volume fraction was calculated as the ratio of the collagen-positive area to the total tissue area. All evaluations were conducted under blinded conditions.

Immunohistochemistry

The sections were placed in a wax-melting box at 60 °C for 1 h, dewaxed with xylene, and rehydrated. A freshly prepared pH 9.0 EDTA antigen retrieval solution was used, and antigen retrieval was carried out by heating in a pressure cooker for 2 min. An endogenous peroxidase blocking agent (ZSG-BIO, PV-9000, Beijing, China) was added and incubated at 37 °C for 10 min. The sections were then washed thrice with PBS buffer for 3 min each time. Primary antibodies against Wnt1 (1:50, 27935-1-AP, Proteintech, Wuhan, China), Sirt1 (1:50, ab189494, Abcam, Cambridge, UK), α-SMA (1:50, 14395-1-AP, Proteintech), and CD31 (1:100, 28083-1-AP, Proteintech) were added and incubated overnight at 4 °C in a refrigerator, followed by PBS washing. Subsequently, the sections were incubated with enhancing solution at room temperature for 20 min followed by PBS washing. The enhanced enzyme-labeled goat anti-mouse/rabbit IgG polymer was applied to the sections and incubated at 37 °C for 20 min, followed by washing with PBS. The Image J software was used to compute the integrated optical density resulting from the DAB chromogenic reaction.

Western Blot Analysis

Renal tissue samples (40 mg) were homogenized in a suitable volume of RIPA lysis buffer supplemented with phosphatase and protease inhibitors at 4 °C. Following thorough grinding, the mixture was centrifuged to collect the supernatant, which was then used for sample preparation. For each well, 30–40 μg of total protein from renal tissue or 20–30 μg from EA.hy926 cells was loaded. The proteins were separated by SDS-PAGE gel electrophoresis, transferred onto a membrane, and blocked with 5% nonfat milk for 2 h. Primary antibodies against p-β-catenin (1:5000, #4176, CST, Danvers USA), β-catenin (1:5000, 66379-1-AP, Proteintech), α-SMA (1:4000, 14395-1-AP, Proteintech), GAPDH (1:10000, 10494-1-AP, Proteintech), Sirt1 (1:1000, ab189494, Abcam), CD31 (1:1000, 28083-1-AP, Proteintech), vimentin (1:2000, 10366-1-AP, Proteintech), and β-actin (1:15000, 66009-1-AP, Proteintech) were applied to the membranes and incubated overnight at 4 °C. Following three washes with TBST for 10 min each, secondary antibodies were added and incubated at room temperature for 2 h with gentle agitation. Following another wash, the chemiluminescent substrate was added for detection. Protein bands were visualized and analyzed semiquantitatively using the Image Lab software (Bio-Rad Laboratories, Hercules, CA, USA).

Cell Culture

EA.hy926, a human umbilical vein endothelial cell fusion cell line, was obtained from Wuhan Procell Life Science & Technology Co., Ltd. The cells were cultured in DMEM (Procell, Wuhan, China) enriched with 10% fetal bovine serum (FBS, Procell) and 1% penicillin/streptomycin (Procell), and incubated at 37 °C and 5% CO_2. The control group received no treatment. The model group was treated with TGF-β1 at concentrations of 5, 10, and 20 ng/mL (MedChemExpress, Monmouth Junction, USA). The LWDHD group was cultured with 5%, 10%, and 20% drug-containing serum. The EX527 (S1541, Selleck, Shanghai, China) group was treated with a concentration of 10 μmol/L, and the SRT1720 (S1129, Selleck) group was treated with a concentration of 4 μmol/L. All groups were cultured for 24 h. Based on the preliminary results, 10 ng/mL TGF-β1 and 10% LWDHD drug-containing serum were selected for subsequent experiments.

Immunofluorescence

Cell climbing slices were placed in 24-well plates, and cells were seeded in the wells. Each group of cells was fixed with 1% paraformaldehyde for 15 min. Subsequently, 5% BSA blocking solution was added and incubated at 25 °C for 30 min. Primary antibodies against Wnt1 (1:50; 27935-1-AP, Proteintech), Sirt1 (1:50; ab189494, Abcam), vimentin (1:100; 10366-1-AP, Proteintech), and CD31 (1:100; 28083-1-AP, Proteintech) were added to each well and incubated overnight at 4 °C in a refrigerator. On the next day, the corresponding secondary antibodies were added and incubated at 25 °C for 1.5 h. DAPI was added for 10 min. The slices were mounted using an antifluorescence quenching agent. The tissue sections were incubated overnight with primary antibodies against CD31 (1:200; 28083-1-AP, Proteintech) and vimentin (1:100; 10366-1-AP, Proteintech). Subsequently, the corresponding fluorescent secondary antibodies were added. Fluorescence images were acquired using an automatic digital slide scanner (3DHISTECH, Budapest, Hungary).

ROS Detection

Cells were seeded in 24-well plates. After the intervention, the existing culture medium was removed, and the cells were washed once with serum-free medium. For ROS detection, the Reactive Oxygen Species Fluorometric Assay Kit (E-BC-K138-F; Elabscience, Wuhan, China) was used. Specifically, 200 μL of the prepared reagent one working solution was added to the wells, followed by incubation at 37 °C in the dark for 40 min. Subsequently, the cells were washed twice or thrice with serum-free medium before obtaining fluorescence images using an automatic digital slide scanner (3DHISTECH).

Statistical Analysis

All quantitative data are presented as the mean ± standard deviation (SD). Normality tests were conducted for all datasets. For data conforming to a normal distribution and exhibiting homogeneity of variance, one-way analysis of variance (ANOVA) was performed, followed by the Tukey post-hoc test. In cases where the data deviated from normality or exhibited heterogeneity of variance, the Kruskal–Wallis test was applied, followed by the Dunn post-hoc test. $P < 0.05$ was considered statistically significant. Statistical graphs were subsequently generated using GraphPad Prism 9.

Results

Determination of the Main Active Components in LWDHD

We quantified the primary active constituents in LWDHD using UHPLC-MS/MS under negative ion mode. By integrating data from the TCMSP database on the chemical profiles of six herbal ingredients, and by comparing retention times with those of standard compounds and through literature search,[19] we identified four key active components: loganin, paeoniflorin, morroniside, and rehmannioside (Figure 1).

Target Prediction and Enrichment Analysis

After removing duplicates from the GenCards database, we identified 51 target genes (Supplementary Table S1). By searching for "Renal fibrosis" in both GenCards and OMIM databases and eliminating duplicates, we obtained 3890

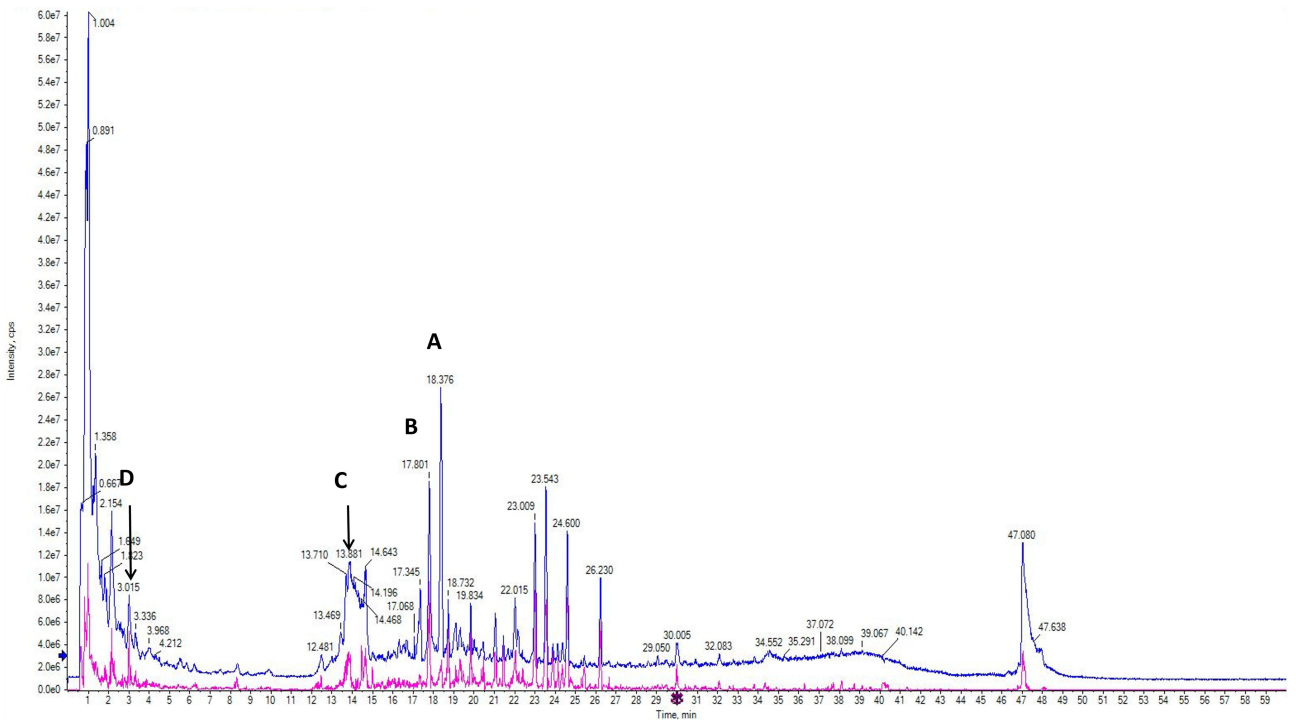

Figure 1 Representative UHPLC-MS/MS analysis of total ion flow (negative ions) for the four main components in LWDHD. (**A**) loganin; (**B**) paeoniflorin; (**C**) morroniside; (**D**) rehmannioside.

target genes (Supplementary Table S2). Using the Venny2.1.0 online tool, we intersected the two sets of target genes and identified 33 common targets (Figure 2A). The generated protein-protein interaction (PPI) network contained 33 nodes and 223 edges (Figure 2B). We applied the degree topology algorithm to screen the top 20 key targets, which were then visualized in a network diagram (Figure 2C). We selected Sirt1 as the key target for further investigation.

The results of GO function and KEGG pathway enrichment analyses indicated that LWDHD affected various biological processes (BP), molecular functions (MF), and cellular components (CC). Specifically, GO function analysis (Figure 2D) revealed that the top 20 key targets of LWDHD in renal fibrosis were primarily involved in both the positive and negative regulation of apoptosis, as well as in the positive regulation of RNA polymerase II transcription and signal transduction. These targets were predominantly localized in the nucleus, cytoplasm, and cytosol, and were associated with molecular functions such as protein binding, enzyme activity, and protein phosphatase activity. KEGG pathway analysis (Figure 2E) demonstrated that the targets were enriched in pathways associated with cancer development, lipid metabolism, and atherosclerosis.

Molecular docking studies revealed that the active components loganin, morroniside, and paeoniflorin had binding energies of −1.28, −0.79, and −1.53 kcal/mol, respectively, with the core target Sirt1 (Figure 2F–H). These findings suggested that all three active components can spontaneously bind to the Sirt1 protein, indicating their potential significance for further research.

LWDHD Ameliorates Renal Fibrosis in Rats

HE staining demonstrated (Figure 3A) that the glomerular structure in the Sham group was well-preserved, with tightly arranged renal tubules and collecting ducts. Whereas, in the UUO group, a significant infiltration of inflammatory cells was observed in the renal interstitium, with numerous renal tubules exhibiting dilation, indicating severe injury. Different doses of LWDHD mitigated renal tubular dilatation and glomerular sclerosis, hence dramatically reducing the degree of renal pathological damage compared with that in the UUO group. Masson trichrome staining (Figure 3B) revealed a marked reduction in blue-stained collagen fibers in the renal interstitium of the LWDHD-treated groups compared with that in the UUO group, indicating a decrease in renal fibrosis. Sirius red staining (Figure 3C) revealed that the UUO

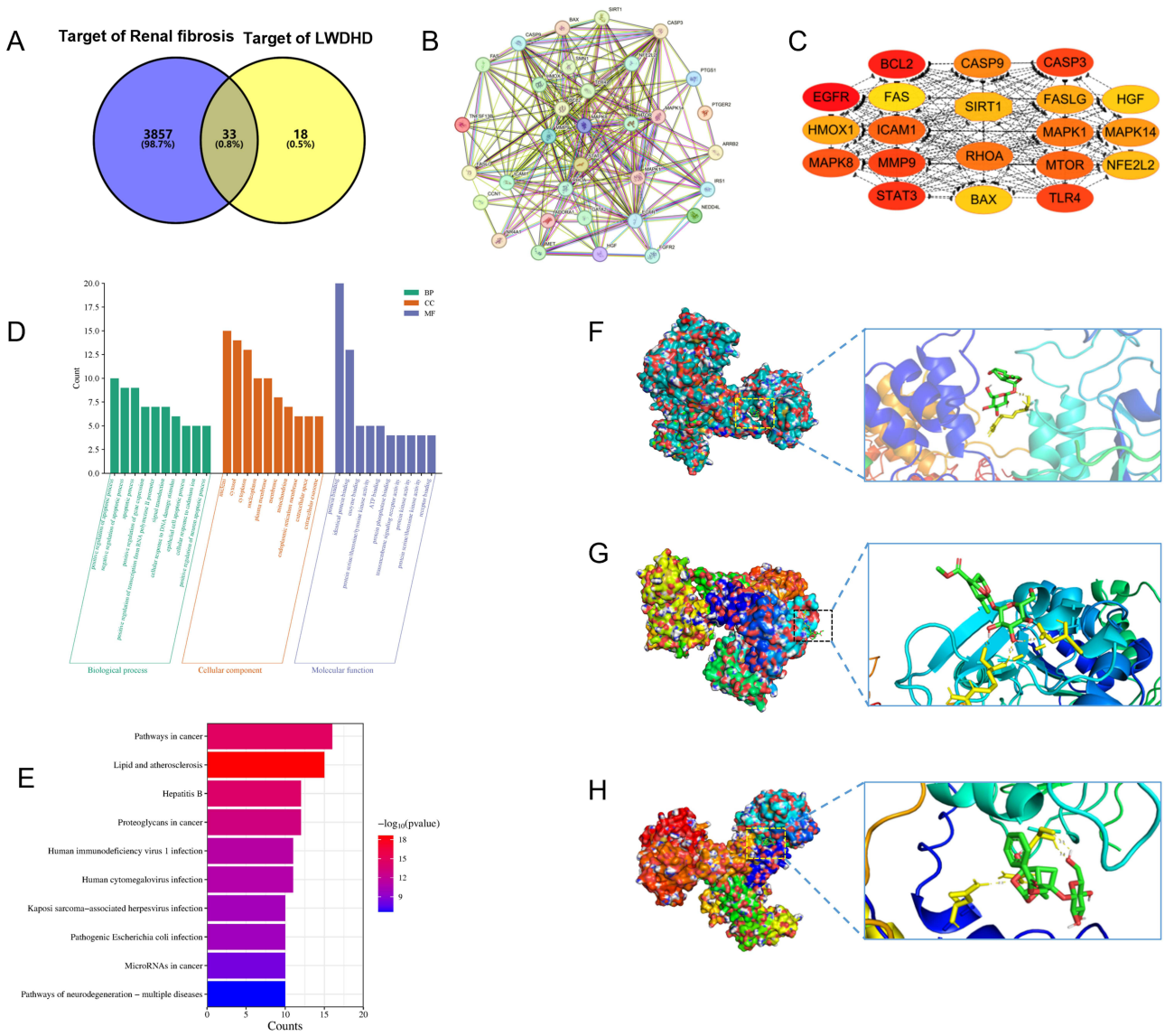

Figure 2 Prediction of key active ingredients, targets, and mechanistic pathways of LWDHD in the treatment of Renal Fibrosis. (**A**) Venn diagram of the key targets of LWDHD in the treatment of renal fibrosis. (**B**) PPI network diagram of intersected targets. (**C**) Top 20 core targets. (**D**) GO functional enrichment analysis. (**E**) KEGG pathway enrichment analysis. (**F**) Molecular docking of the active compound Sirt1-loganin. (**G**) Molecular docking of the active compound Sirt1-morroniside. (**H**) Molecular docking of the active compound Sirt1-paeoniflorin.

group exhibited a significant increase in the content of red-stained collagen fibers within the renal tubular interstitium, which were widely distributed in patchy or cord-like patterns. In the LWDHD-treated groups, the amount of red-stained collagen fibers was notably reduced. These findings suggested that LWDHD exerts an intervention effect on renal fibrosis caused by ureteral obstruction in rats, thereby protecting renal function.

LWDHD Regulates Sirt1 Expression, Inhibits the Activation of the Wnt/β-Catenin Signaling Pathway, and Suppresses Renal Fibrosis

Immunohistochemical analysis demonstrated that Sirt1 expression was strong in the capillary endothelial cells and glomeruli of the Sham group, significantly reduced in the UUO group, whereas progressively increased following treatment with different doses of LWDHD. Conversely, Wnt1 expression was low in the Sham group, markedly elevated in the UUO group, and dose-dependently decreased in the LWDHD-treated groups. The expression pattern of CD31 mirrored that of Sirt1, whereas α-SMA expression paralleled that of Wnt1 (Figure 4A–D and A1–D1). Co-staining

https://doi.org/10.2147/DDDT.S517938

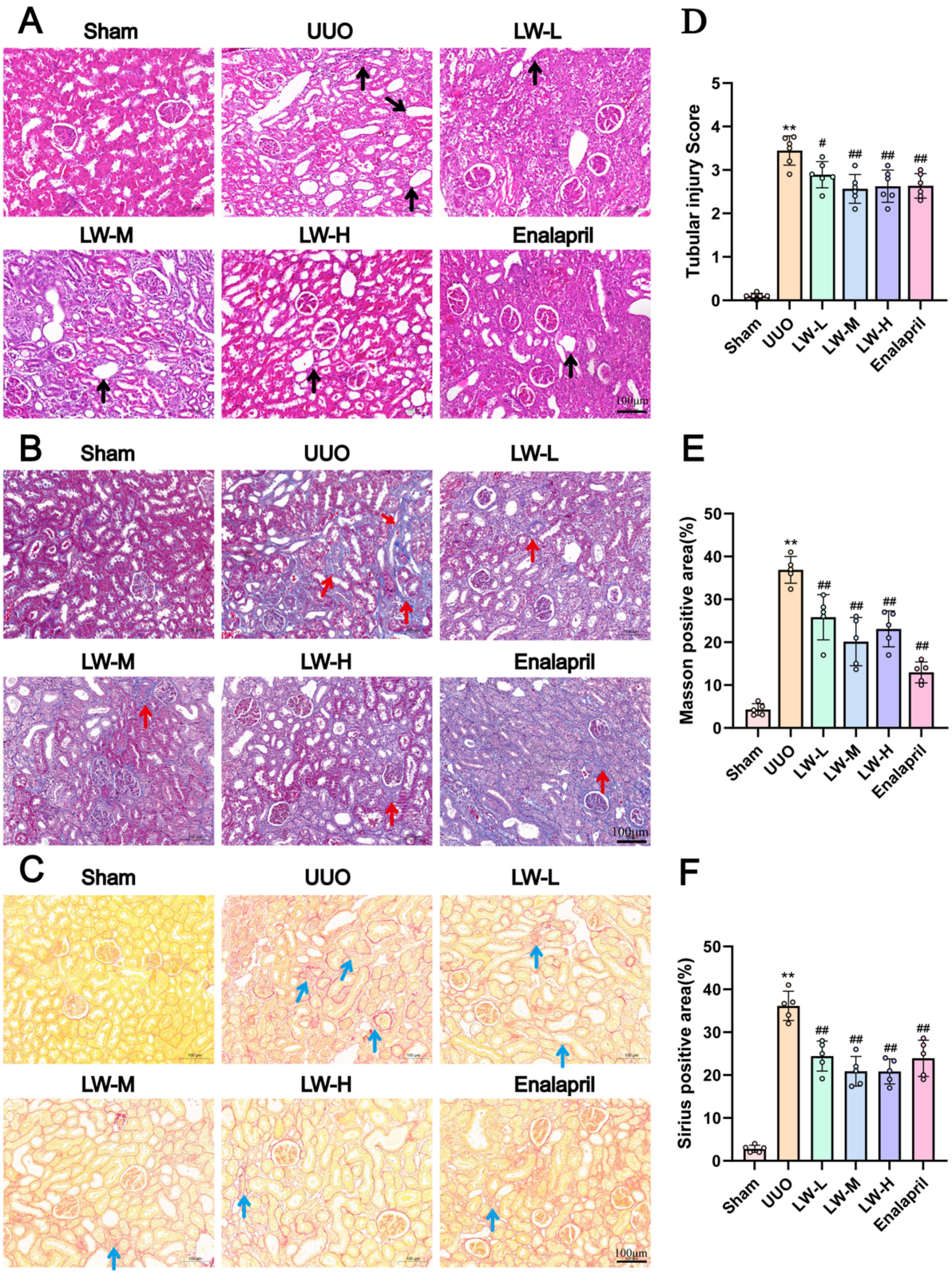

Figure 3 LWDHD alleviated renal injury and extracellular matrix accumulation. (**A**) HE staining of renal tissues in each group; black arrows indicate inflammatory cell infiltration and renal tubular dilation (scale bar = 100 μm). (**B**) Representative images of Masson trichrome staining of renal tissues in each group; red arrows indicate collagen fiber deposition (scale bar = 100 μm). (**C**) Representative images of Sirius Red staining of renal tissues in each group; blue arrows indicate collagen fiber deposition (scale bar = 100 μm). (**D**) Renal tubular injury scores (N = 6). (**E** and **F**) Positive proportions of collagen fibers (N = 5). *P < 0.05, **P < 0.01 vs sham group; #P < 0.05, ##P < 0.01 vs UUO group.

 https://doi.org/10.2147/DDDT.S517938

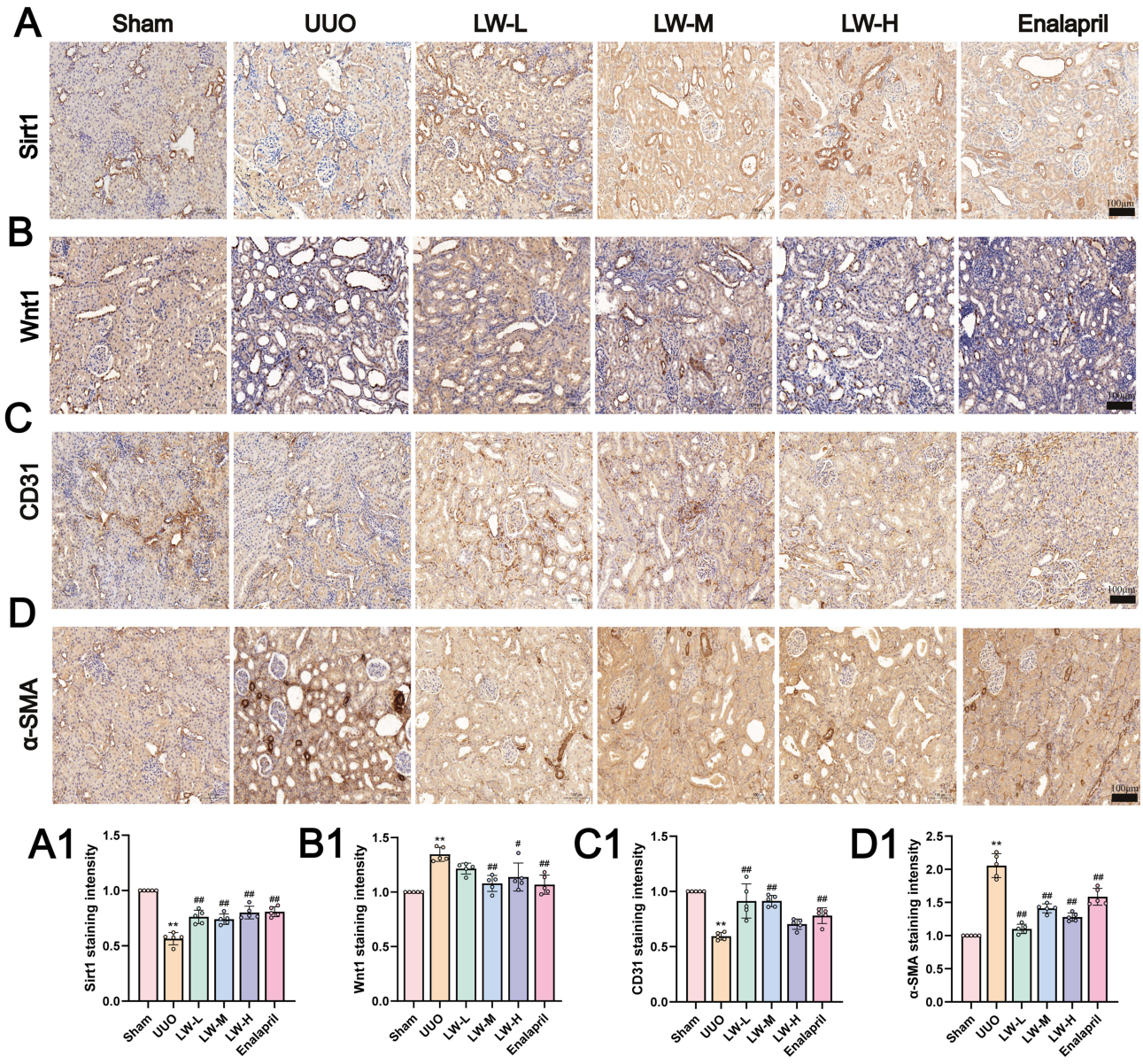

Figure 4 LWDHD increases the expression of Sirt1, inhibits the activation of the Wnt/β-catenin pathway, and alleviates renal fibrosis. (**A**–**D**) Immunohistochemical staining of kidney tissue for Sirt1, Wnt1, CD31, and α-SMA (scale bar = 100 μm). (**A1**–**D1**) Semiquantitative analysis of the Sirt1, Wnt1, CD31, and α-SMA positive staining area (N = 5). $^{*}P < 0.05$, $^{**}P < 0.01$ vs sham; $^{\#}P < 0.05$, $^{\#\#}P < 0.01$ vs UUO.

analysis revealed that, in the UUO group, the fluorescence intensity of CD31 was decreased, whereas that of vimentin was increased, indicating the occurrence of EndMT. In contrast, following LWDHD intervention, the expression of CD31 was significantly upregulated, whereas the increase in vimentin expression was effectively suppressed (Figure 5A–C).

Western blot analysis confirmed that LWDHD upregulated CD31 protein levels, whereas downregulated the expression of Wnt1, vimentin, and α-SMA (Figure 5D–H). Collectively, these results indicated that LWDHD boosts Sirt1 expression, inhibits the activation of the Wnt/β-catenin signaling pathway, and exhibits an antagonistic action against renal fibrosis.

LWDHD Alleviates TGF-β1-Induced EndMT and Increases Sirt1 Expression

To investigate the effect of different concentrations of TGF-β1 on EndMT in EA.hy926 cells, we exposed the cells to 5, 10, and 20 ng/mL of TGF-β1 for 24 h. We found that TGF-β1 treatment notably reduced CD31 protein expression,

https://doi.org/10.2147/DDDT.S517938

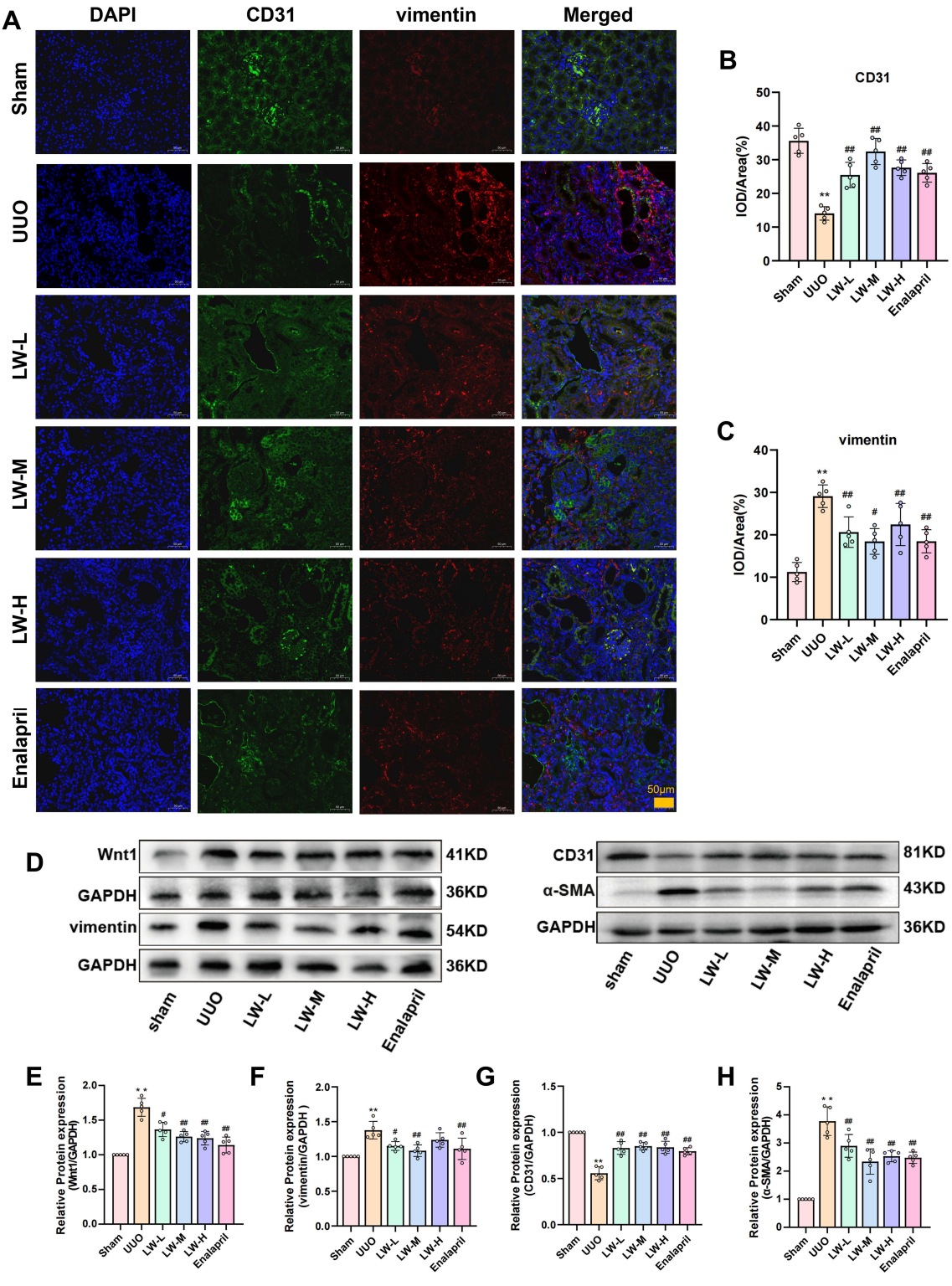

Figure 5 LWDHD inhibits the Wnt/β-catenin pathway and renal EndMT. (**A**–**C**) Immunofluorescence staining and fluorescence quantitative analysis of CD31 and vimentin in renal tissues (N = 5). (**D**) Protein expression of Wnt1, vimentin, CD31, and α-SMA in renal tissues. (**E**–**H**) Quantitative results of Wnt1, vimentin, CD31, and α-SMA levels. (N = 5). $^{*}P < 0.05$, $^{**}P < 0.01$ vs sham; $^{\#}P < 0.05$, $^{\#\#}P < 0.01$ vs UUO.

 https://doi.org/10.2147/DDDT.S517938

whereas elevated vimentin and collagen I protein levels (Figure 6A–D), thereby promoting EndMT. Based on these findings, we selected the concentration of 10 ng/mL TGF-β1 for subsequent experiments ($P < 0.05$). Next, we treated EA.hy926 cells with serum containing 5%, 10%, and 20% LWDHD for 24 h. Microscopic observations revealed that cells in the Control group exhibited a typical cobblestone-like morphology with regular arrangement (Figure 6E). In contrast, cells in the TGF-β1 group displayed elongated, spindle-shaped morphology characteristic of fibroblasts, with a reduced cell number. Treatment with different doses of LWDHD mitigated these morphological changes without significantly altering cell numbers. Western blot analysis revealed that, compared with the Control group, the TGF-β1 group exhibited decreased expression of Sirt1, p-β-catenin, and CD31. However, treatment with LWDHD reversed this trend by upregulating their expression. Conversely, vimentin expression was increased in the TGF-β1 group, whereas it was

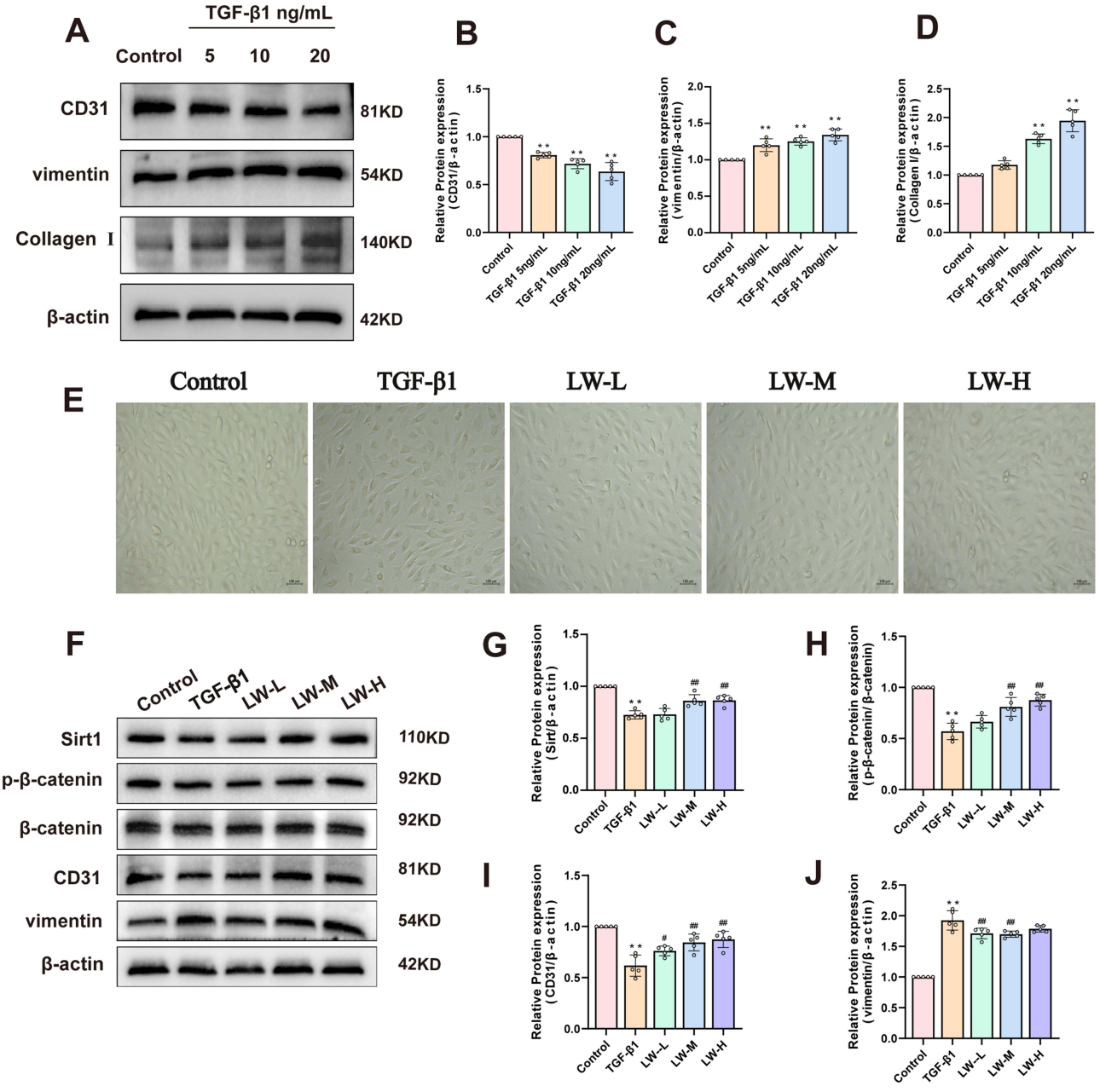

Figure 6 LWDHD increases Sirt1 expression in EA.hy926 cells, inhibits the activation of the Wnt/β-catenin pathway, and alleviates renal fibrosis. (**A**–**D**) Western blot results and quantitative analysis of the expression of CD31, vimentin, and Collagen I in EA.hy926 cells (N = 5). (**E**) Microscopic morphology observations (scale bar = 100 μm). (**F**–**J**) Western blot results and quantitative analysis of the expression of Sirt1, p-β-catenin, CD31, and vimentin (N = 5). Statistical significance is denoted as follows: $^{*}P < 0.05$, $^{**}P < 0.01$ vs control; $^{\#}P < 0.05$, $^{\#\#}P < 0.01$ vs TGF-β1.

https://doi.org/10.2147/DDDT.S517938

decreased in the LWDHD-treated groups (Figure 6F–J). These observations suggested that LWDHD can effectively counteract the TGF-β1-induced EndMT.

LWDHD Targets Sirt1 to Inhibit Wnt/β-Catenin Activation and Suppress EndMT

Sirt1 is ubiquitously expressed and plays a pivotal role in modulating oxidative stress by hindering the abnormal ROS accumulation within cells. To further verify that LWDHD targets Sirt1 to inhibit Wnt/β-catenin, we treated EA.hy926 cells with the Sirt1 inhibitor EX527 and agonist SRT1720 for 24 h. Western blot analysis demonstrated that compared with the TGF-β1 group, the TGF-β1+LWDHD and TGF-β1+SRT1720 groups exhibited increased expression of Sirt1, p-β-catenin, and CD31 proteins, whereas the expression of vimentin was decreased, thereby inhibiting EndMT. In contrast, the TGF-β1 +EX527 group displayed significantly lower expression of Sirt1, p-β-catenin, and CD31 proteins, along with increased expression of vimentin and collagen I. Notably, in the TGF-β1+LWDHD+EX527 group, the reduction in protein expression was partially reversed, whereas the significant increase in the levels of fibrosis-related proteins was inhibited. These findings indicated that LWDHD and SRT1720 enhance Sirt1 expression (Figure 7A–F), thereby inhibiting Wnt/β-catenin pathway activation, thus exerting an antifibrotic effect. ROS detection (Figure 7G and H) demonstrated that ROS fluorescence intensity was markedly elevated in the TGF-β1 group, indicating elevated ROS levels. Compared with the TGF-β1 group, both the TGF-β1+LWDHD and TGF-β1+SRT1720 groups exhibited reduced ROS fluorescence, suggesting decreased ROS production. Conversely, the EX527-treated group exhibited increased ROS accumulation, which was partially reversed in the TGF-β1+LWDHD+EX527 group. These findings demonstrated that LWDHD upregulates Sirt1 expression, hence reducing ROS accumulation and alleviating cellular damage. Immunofluorescence staining (Figure 8A–D) further confirmed that LWDHD increased the expression of Sirt1 and CD31, reduced the expression of pathway protein Wnt1 and fibrosis-related proteins vimentin, thereby inhibiting EndMT progression. Collectively, these findings suggested that LWDHD exerts its antifibrotic effects by increasing Sirt1 expression and inhibiting Wnt/β-catenin pathway activation, thus suppressing EndMT.

Discussion

The kidney is a crucial organ in the human body; yet, the prevalence of CKD, which affects approximately 10% of the global adult population, is increasing annually.[31] Comprehensive research into the mechanisms of RF is crucial for developing innovative prevention and treatment strategies for CKD. The UUO model is widely recognized as a standard model for RIF and pathological alterations in peritubular capillaries.[18,32] Moreover, renal endothelial cells not only serve as the glomerular filtration barrier while supporting capillary structure but also play a pivotal role in the progression of kidney diseases, particularly in RF. Research has indicated that during RF, endothelial cells undergo EndMT,[6,33] losing their adhesion properties and transforming into highly invasive and migratory mesenchymal cells. Oxidative stress and inflammation can induce local hypoxia, which is a critical factor contributing to CKD development.[34,35]

In recent years, TCM has exhibited considerable potential in the management and treatment of CKD. Certain natural compounds, such as poricoic acid A, have been shown to inhibit RIF by modulating the Sirtuin family and Wnt/β-catenin signaling pathways.[36] Additionally, diosgenin upregulates Sirt6 expression, mitigates lipid accumulation, and protects podocytes from damage in diabetic nephropathy.[37] TCM has demonstrated significant therapeutic potential in the management of kidney diseases by targeting the Sirtuin family and modulating the Wnt/β-catenin signaling pathway.[38] LWDHD, a classical TCM prescription characterized by its “three tonics and three purgatives” formula, is widely used for patients with kidney qi deficiency. Moreover, it exhibits protective effects on multiple organ systems, including the liver, nervous system, cardiovascular system, and skeletal system.[39] Pertinent research has indicated that Liuwei Dihuang Pills exhibit therapeutic efficacy in the management of osteoporosis associated with diabetic nephropathy by down-regulating the KDM7A protein and modulating the Wnt/β-catenin signaling pathway.[40] Studies have demonstrated that LWDHD increases superoxide dismutase (SOD) and nitric oxide synthase (NOS) levels while reducing malondialdehyde (MDA) concentration, thereby alleviating lipid peroxidation damage. Its multicomponent and multitarget nature contributes significantly to its antioxidative properties.[41]

The present study identified Sirt1 as a pivotal target that interacts directly with the active constituents of LWDHD, as established through UHPLC-MS/MS analysis and network pharmacology approaches. Sirt1 mitigates the abnormal accumulation of ROS in cells, inhibits oxidative stress in vascular endothelial cells, and improves endothelial

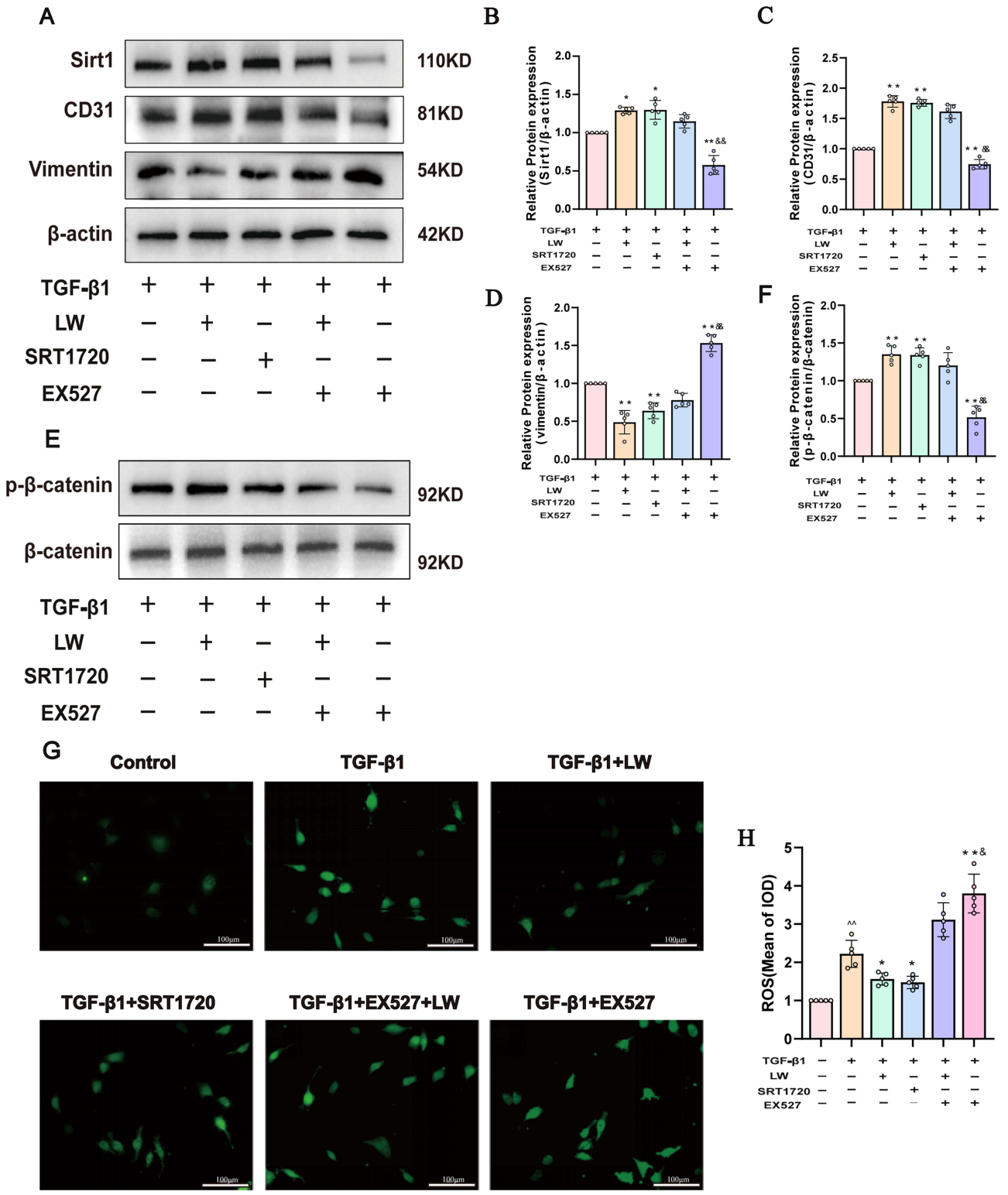

Figure 7 LWDHD increases intracellular Sirt1 expression, inhibits oxidative stress, suppresses activation of the Wnt/β-catenin pathway, and reduces damage. (**A**–**F**) Western blot results and quantitative analysis of intracellular expression of Sirt1, CD31, vimentin, and p-β-catenin (N = 5). (**G** and **H**) Average fluorescence area of ROS in each group of cells and quantitative analysis (N = 5), scale bar = 100 μm. $^{\wedge\wedge}P < 0.01$ vs control; $^{*}P < 0.05$, $^{**}P < 0.01$ vs TGF-β1; $^{\#}P < 0.05$, $^{\#\#}P < 0.01$ vs TGF-β1+LW; $^{\&}P < 0.05$, $^{\&\&}P < 0.01$ vs TGF-β1+EX527+LW.

https://doi.org/10.2147/DDDT.S517938

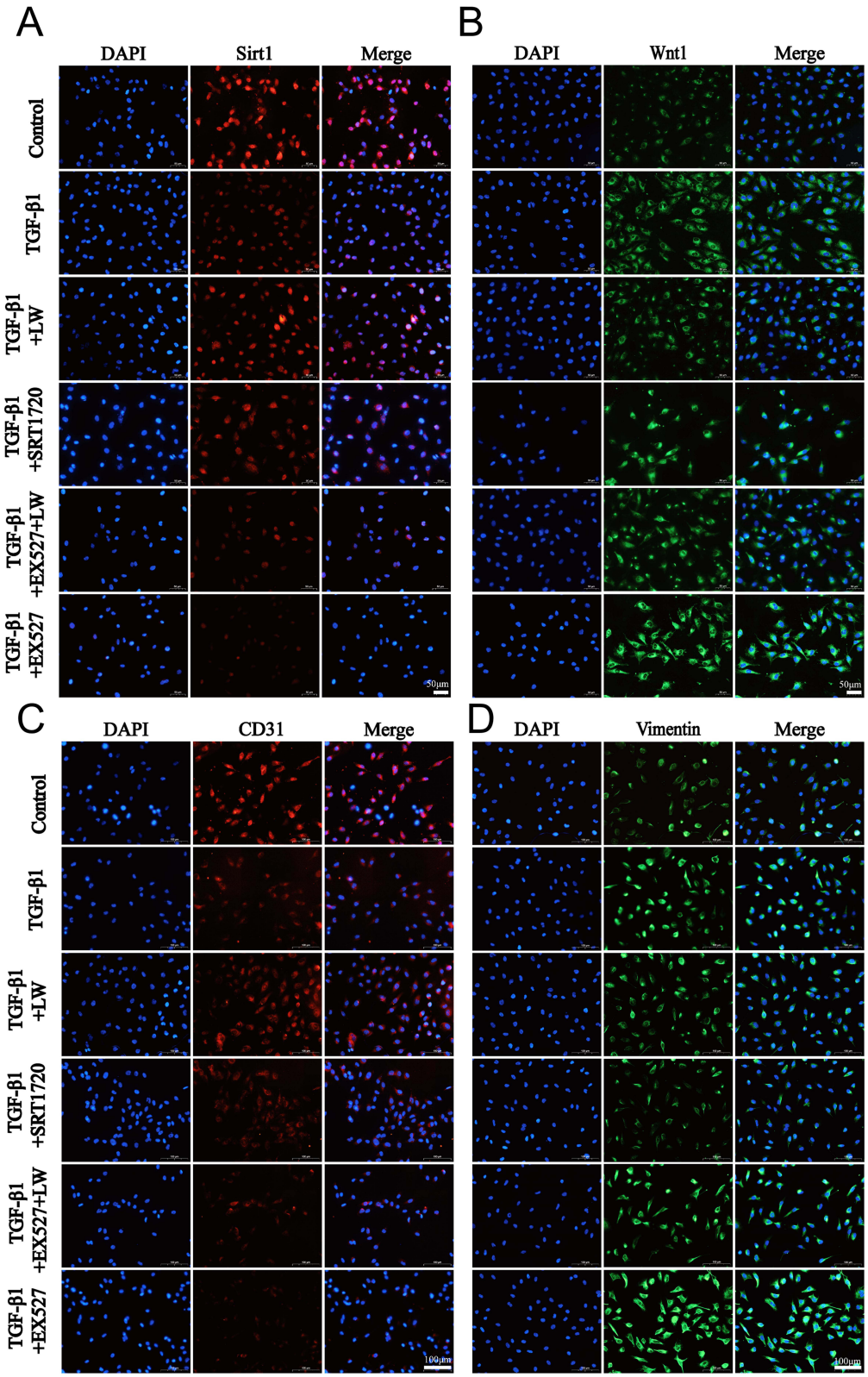

Figure 8 LWDHD inhibits EndMT in EA.hy926 cells. (**A–D**) Immunofluorescence results of Sirt1, Wnt1, CD31, and vimentin in each group of cells. Sirt1 and Wnt1, scale bar = 50 μm; CD31 and vimentin, scale bar = 100 μm.

dysfunction.[42] Sirt1 plays a critical role in CKD pathogenesis.[43,44] Our findings indicated that, compared with the UUO group, the LWDHD-treated group exhibited reduced renal tubular dilation, improved glomerular atrophy, decreased inflammatory cell infiltration, and overall amelioration of kidney pathology as indicated via HE, Masson, and Sirius Red staining. In both UUO rats and TGF-β1-induced EA.hy926 cells, Sirt1 expression was downregulated, further supporting its critical role in RF. EndMT development involves multiple signaling pathways, such as TGF-β, Notch, and Wnt/β-catenin,[45,46] The regulation of the Wnt/β-catenin signaling pathway has exhibited significant therapeutic potential in the management of CKD and cardiorenal syndrome.[47,48] Consequently, we identified the Wnt/β-catenin signaling pathway as the primary focus of our research. Furthermore, prior studies have indicated that Sirt1 suppresses the activation of the Wnt/β-catenin pathway.[49] To further verify whether LWDHD can regulate Sirt1 and thereby inhibit the Wnt/β-catenin pathway, we conducted in vitro experiments using the Sirt1 inhibitor EX527 and agonist SRT1720.[50,51] Our results showed that LWDHD reversed the inhibitory effects of TGF-β1 and EX527 on Sirt1, increased β-catenin phosphorylation, reduced cytoplasmic β-catenin accumulation, and consequently upregulated the expression of the endothelial marker CD31 while downregulating that of the fibrosis-related protein vimentin. Additionally, LWDHD inhibited intracellular ROS accumulation, thereby reducing oxidative stress-induced cellular damage. The aforementioned results indicated that LWDHD can upregulate the expression of Sirt1, consequently suppressing the activation of the Wnt/β-catenin pathway, thus mitigating EndMT progression. The findings of the present study offer novel insights for the clinical prevention and management of CKD and contribute toward mitigating the onset and progression of this condition.

However, our study had certain limitations. The Wnt/β-catenin pathway was selected based on extensive literature search to investigate the regulatory effect of Sirt1, rather than selecting the top-ranked signaling pathways enriched in KEGG analysis. Therefore, this approach may have introduced potential constraints into the research findings. Additionally, other predicted key targets and pathways were not investigated; a more comprehensive and systematic exploration of these targets should be performed in future studies. Furthermore, while examining the role of Sirt1, we did not perform gene-level knockdown experiments, nor did we fully validate the upstream and downstream relationships of the Wnt/β-catenin pathway using specific agonists and inhibitors. Consequently, considerable scope remains for further investigation in our study. Future research should integrate gene-level manipulations involving Sirt1 and the Wnt/β-catenin signaling pathway. Moreover, a deeper and more holistic mechanistic understanding is required for the prevention and treatment of CKD based on TCM.

Conclusion

In conclusion, our study demonstrated that LWDHD has a protective effect on the structure and function of the kidneys. Effectively delay the progression of EndMT. These beneficial effects may be attributed to the upregulation of Sirt1 expression, which subsequently inhibits Wnt/β-catenin pathway activation, leading to an antifibrotic outcome.

Abbreviations

Sirt1, Silent information regulator 1; CKD, chronic kidney disease; RF, Renal fibrosis; LWDHD, Liu Wei Di Huang Decoction; ROS, reactive oxygen species; TGF-β1, transforming growth factor-β1; UUO, Unilateral ureteral obstruction.

Data Sharing Statement

Some materials and methods, including the preparation of drug-containing serum, are detailed in Supplementary.

Funding

This research was supported by A Project Supported by Scientific Research Fund of Hunan Provincial Education Department (21A0242), Hunan University of Traditional Chinese Medicine Graduate Innovation Project (2022CX182), Hunan Provincial Natural Science Foundation Project (2025JJ90041).

Disclosure

No potential conflicts of interest were declared by the authors.

References

1. Luyckx VA, Al-Aly Z, Bello AK, et al. Sustainable development goals relevant to kidney health: an update on progress. *Nat Rev Nephrol*. 2021;17(1):15–32. doi:10.1038/s41581-020-00363-6
2. Foreman KJ, Marquez N, Dolgert A, et al. Forecasting life expectancy, years of life lost, and all-cause and cause-specific mortality for 250 causes of death: reference and alternative scenarios for 2016-40 for 195 countries and territories. *Lancet*. 2018;392(10159):2052–2090. doi:10.1016/S0140-6736(18)31694-5
3. Humphreys BD. Mechanisms of Renal Fibrosis. *Annu Rev Physiol*. 2018;80:309–326. doi:10.1146/annurev-physiol-022516-034227
4. Djudjaj S, Boor P. Cellular and molecular mechanisms of kidney fibrosis. *Mol Aspects Med*. 2019;65:16–36. doi:10.1016/j.mam.2018.06.002
5. Liu Y, Wu J, Liang S, et al. Guben Xiezhuo Decoction inhibits M1 polarization through the Raf1/p-Elk1 signaling axis to attenuate renal interstitial fibrosis. *J Ethnopharmacol*. 2024;319(Pt 2):117189. doi:10.1016/j.jep.2023.117189
6. Cruz-Solbes AS, Youker K. Epithelial to Mesenchymal Transition (EMT) and Endothelial to Mesenchymal Transition (EndMT): role and implications in kidney fibrosis. *Results Probl Cell Differ*. 2017;60:345–372. doi:10.1007/978-3-319-51436-9_13
7. Curci C, Castellano G, Stasi A, et al. Endothelial-to-mesenchymal transition and renal fibrosis in ischaemia/reperfusion injury are mediated by complement anaphylatoxins and Akt pathway. *Nephrol Dial Transplant*. 2014;29(4):799–808. doi:10.1093/ndt/gft516
8. Lovisa S, Fletcher-Sananikone E, Sugimoto H, et al. Endothelial-to-mesenchymal transition compromises vascular integrity to induce Myc-mediated metabolic reprogramming in kidney fibrosis. *Sci Signal*. 2020;13(635):eaaz2597. doi:10.1126/scisignal.aaz2597
9. Piera-Velazquez S, Jimenez SA. Endothelial to mesenchymal transition: role in physiology and in the pathogenesis of human diseases. *Physiol Rev*. 2019;99(2):1281–1324. doi:10.1152/physrev.00021.2018
10. Staal FJ, Luis TC, Tiemessen MM. WNT signalling in the immune system: WNT is spreading its wings. *Nat Rev Immunol*. 2008;8(8):581–593. doi:10.1038/nri2360
11. Li SS, Sun Q, Hua MR, et al. Targeting the Wnt/β-Catenin signaling pathway as a potential therapeutic strategy in renal tubulointerstitial fibrosis. *Front Pharmacol*. 2021;12:719880. doi:10.3389/fphar.2021.719880
12. Yan J, Wang J, He JC, et al. Sirtuin 1 in chronic kidney disease and therapeutic potential of targeting sirtuin 1. *Front Endocrinol*. 2022;13:917773. doi:10.3389/fendo.2022.917773
13. Jin J, Li W, Wang T, et al. Loss of proximal tubular sirtuin 6 aggravates unilateral ureteral obstruction-induced tubulointerstitial inflammation and fibrosis by regulation of β-catenin acetylation. *Cells*. 2022;11(9):1477. doi:10.3390/cells11091477
14. Cai J, Liu Z, Huang X, et al. The deacetylase sirtuin 6 protects against kidney fibrosis by epigenetically blocking β-catenin target gene expression. *Kidney Int*. 2020;97(1):106–118. doi:10.1016/j.kint.2019.08.028
15. Miao H, Wang YN, Su W, et al. Sirtuin 6 protects against podocyte injury by blocking the renin-angiotensin system by inhibiting the Wnt1/β-catenin pathway. *Acta Pharmacol Sin*. 2024;45(1):137–149. doi:10.1038/s41401-023-01148-w
16. Singh V, Ubaid S. Role of Silent Information Regulator 1 (SIRT1) in regulating oxidative stress and inflammation. *Inflammation*. 2020;43(5):1589–1598. doi:10.1007/s10753-020-01242-9
17. Yang S, Lian G. ROS and diseases: role in metabolism and energy supply. *Mol Cell Biochem*. 2020;467(1–2):1–12. doi:10.1007/s11010-019-03667-9
18. Wang Y, Zuo B, Wang N, et al. Calcium dobesilate mediates renal interstitial fibrosis and delay renal peritubular capillary loss through Sirt1/p53 signaling pathway. *Biomed Pharmacother*. 2020;132:110798. doi:10.1016/j.biopha.2020.110798
19. Zhou L, Wu K, Gao Y, et al. Piperlonguminine attenuates renal fibrosis by inhibiting TRPC6. *J Ethnopharmacol*. 2023;313:116561. doi:10.1016/j.jep.2023.116561
20. Liang X, Li H, Li S. A novel network pharmacology approach to analyse traditional herbal formulae: the Liu-Wei-Di-Huang pill as a case study. *Mol Biosyst*. 2014;10(5):1014–1022. doi:10.1039/c3mb70507b
21. Shi R, Wang Y, An X, et al. Efficacy of co-administration of Liuwei Dihuang pills and Ginkgo biloba tablets on albuminuria in type 2 diabetes: a 24-month, multicenter, double-blind, placebo-controlled, randomized clinical trial. *Front Endocrinol*. 2019;10:100. doi:10.3389/fendo.2019.00100
22. Pan J, Jiang Y, Huang Y, et al. Liuwei Dihuang decoction drug-containing serum attenuates transforming growth factor-β1-induced epithelial-mesenchymal transition in HK-2 cells by inhibiting NF-κB/snail signaling pathway. *Curr Pharm Biotechnol*. 2023;24(12):1589–1602. doi:10.2174/1389201024666230228100718
23. Guo ZY, Wu X, Zhang SJ, et al. Poria cocos: traditional uses, triterpenoid components and their renoprotective pharmacology. *Acta Pharmacol Sin*. 2025;46(4):836–851. doi:10.1038/s41401-024-01404-7
24. Tang Y, Wan F, Tang X, et al. Celastrol attenuates diabetic nephropathy by upregulating SIRT1-mediated inhibition of EZH2related wnt/β-catenin signaling. *Int Immunopharmacol*. 2023;122:110584. doi:10.1016/j.intimp.2023.110584
25. Jiang X, Zhou L, Zuo L, et al. Pharmacokinetics and metabolism research of shenkang injection in rats based on UHPLC-MS/MS and UHPLC-Q-Orbitrap HRMS. *Drug Des Devel Ther*. 2020;14:1837–1850. doi:10.2147/DDDT.S235646
26. Huang X, Peng Y, Lu L, et al. Huangqi-Danshen decoction against renal fibrosis in UUO mice via TGF-β1 induced downstream signaling pathway. *Drug Des Devel Ther*. 2024;18:4119–4134. doi:10.2147/DDDT.S457100
27. Jin R, Pei H, Yue F, et al. Network pharmacology combined with metabolomics reveals the mechanism of Yangxuerongjin pill against type 2 diabetic peripheral neuropathy in rats. *Drug Des Devel Ther*. 2025;19:325–347. doi:10.2147/DDDT.S473146
28. Chen J, Li D. Telbivudine attenuates UUO-induced renal fibrosis via TGF-β/Smad and NF-κB signaling. *Int Immunopharmacol*. 2018;55:1–8. doi:10.1016/j.intimp.2017.11.043
29. Tang Q, Wu H, Zhang X, et al. Effects of Liuwei Dihua Tang on the expression of PHD2 and HIF-1α in rats with chronic renal failure. *Beijing Univ Tradit Chin Med*. 2017;40(4):290–296. (in Chinese).
30. Ueno T, Nakashima A, Doi S, et al. Mesenchymal stem cells ameliorate experimental peritoneal fibrosis by suppressing inflammation and inhibiting TGF-β1 signaling. *Kidney Int*. 2013;84(2):297–307. doi:10.1038/ki.2013.81
31. Lohia S, Vlahou A, Zoidakis J. Microbiome in Chronic Kidney Disease (CKD): an omics perspective. *Toxins*. 2022;14(3):176. doi:10.3390/toxins14030176
32. Guerrot D, Dussaule JC, Kavvadas P, et al. Progression of renal fibrosis: the underestimated role of endothelial alterations. *Fibrogenesis Tissue Repair*. 2012;5(Suppl 1):S15. doi:10.1186/1755-1536-5-S1-S15

33. Pardali E, Sanchez-Duffhues G, Gomez-Puerto MC, et al. TGF-β-induced endothelial-mesenchymal transition in fibrotic diseases. *Int J Mol Sci*. 2017;18(10):2157. doi:10.3390/ijms18102157
34. Ebert T, Neytchev O, Witasp A, et al. Inflammation and oxidative stress in chronic kidney disease and dialysis patients. *Antioxid Redox Signal*. 2021;35(17):1426–1448. doi:10.1089/ars.2020.8184
35. Klionsky DJ, Abdel-Aziz AK, Abdelfatah S, et al. Guidelines for the use and interpretation of assays for monitoring autophagy (4th edition)(1). *Autophagy*. 2021;17(1):1–382. doi:10.1080/15548627.2020.1797280
36. Chen DQ, Chen L, Guo Y, et al. Poricoic acid A suppresses renal fibroblast activation and interstitial fibrosis in UUO rats via upregulating Sirt3 and promoting β-catenin K49 deacetylation. *Acta Pharmacol Sin*. 2023;44(5):1038–1050. doi:10.1038/s41401-022-01026-x
37. Wang Z, Wu Q, Wang H, et al. Diosgenin protects against podocyte injury in early phase of diabetic nephropathy through regulating SIRT6. *Phytomedicine*. 2022;104:154276. doi:10.1016/j.phymed.2022.154276
38. Jin Q, Liu T, Ma F, et al. Therapeutic application of traditional Chinese medicine in kidney disease: sirtuins as potential targets. *Biomed Pharmacother*. 2023;167:115499. doi:10.1016/j.biopha.2023.115499
39. Chan KW, Chow TY, Yu KY, et al. Effectiveness of integrative Chinese-Western medicine for chronic kidney disease and diabetes: a retrospective cohort study. *Am J Chin Med*. 2022;50(2):371–388. doi:10.1142/S0192415X2250015X
40. Liu MM, Dong R, Hua Z, et al. Therapeutic potential of Liuwei Dihuang pill against KDM7A and Wnt/β-catenin signaling pathway in diabetic nephropathy-related osteoporosis. *Biosci Rep*. 2020;40(9):BSR20201778. doi:10.1042/BSR20201778
41. Xu ZJ, Shu S, Li ZJ, et al. Liuwei Dihuang pill treats diabetic nephropathy in rats by inhibiting of TGF-β/SMADS, MAPK, and NF-kB and upregulating expression of cytoglobin in renal tissues. *Medicine*. 2017;96(3):e5879. doi:10.1097/MD.0000000000005879
42. Zhang W, Huang Q, Zeng Z, et al. Sirt1 inhibits oxidative stress in vascular endothelial cells. *Oxid Med Cell Longev*. 2017;2017:7543973. doi:10.1155/2017/7543973
43. Chuang PY, Cai W, Li X, et al. Reduction in podocyte SIRT1 accelerates kidney injury in aging mice. *Am J Physiol Renal Physiol*. 2017;313(3):F621–F628. doi:10.1152/ajprenal.00255.2017
44. Ogura Y, Kitada M, Koya D. Sirtuins and renal oxidative stress. *Antioxidants*. 2021;10(8):1198. doi:10.3390/antiox10081198
45. Li L, Chen L, Zang J, et al. C3a and C5a receptor antagonists ameliorate endothelial-myofibroblast transition via the Wnt/β-catenin signaling pathway in diabetic kidney disease. *Metabolism*. 2015;64(5):597–610. doi:10.1016/j.metabol.2015.01.014
46. Wang W, Wang Z, Tian D, et al. Integrin β3 mediates the endothelial-to-mesenchymal transition via the notch pathway. *Cell Physiol Biochem*. 2018;49(3):985. doi:10.1159/000493229
47. Zhao BR, Hu XR, Wang WD, et al. Cardiorenal syndrome: clinical diagnosis, molecular mechanisms and therapeutic strategies. *Acta Pharmacol Sin*. 2025;46(6):1539–1555. doi:10.1038/s41401-025-01476-z
48. Chen Y, Xue C. Cross-talk of renal cells through WNT signal transduction in the development of fibrotic kidneys. *Front Cell Dev Biol*. 2024;12:1517181. doi:10.3389/fcell.2024.1517181
49. Hao Y, Ren Z, Yu L, et al. p300 arrests intervertebral disc degeneration by regulating the FOXO3/Sirt1/Wnt/β-catenin axis. *Aging Cell*. 2022;21(8):e13677. doi:10.1111/acel.13677
50. Zhang W, Zhang Y, Guo X, et al. Sirt1 protects endothelial cells against LPS-induced barrier dysfunction. *Oxid Med Cell Longev*. 2017;2017:4082102. doi:10.1155/2017/4082102
51. Du L, Qian X, Li Y, et al. Sirt1 inhibits renal tubular cell epithelial-mesenchymal transition through YY1 deacetylation in diabetic nephropathy. *Acta Pharmacol Sin*. 2021;42(2):242–251. doi:10.1038/s41401-020-0450-2